COLD SPRING HARBOR
Molecular Case Studies

RESEARCH REPORT

Two different, mutually exclusively distributed, *TP53* mutations in ovarian and peritoneal tumor tissues of a serous ovarian cancer patient: indicative for tumor origin?

Nyamdelger Sukhbaatar,[1] Anna Bachmayr-Heyda,[1] Katharina Auer,[1] Stefanie Aust,[1] Simon Deycmar,[1] Reinhard Horvat,[2] and Dietmar Pils[3,4]

[1]Department of Obstetrics and Gynecology, Medical University of Vienna, A-1090 Vienna, Austria; [2]Department of Pathology, Medical University of Vienna, A-1090 Vienna, Austria; [3]Section for Clinical Biometrics, Center for Medical Statistics, Informatics, and Intelligent Systems (CeMSIIS), Medical University of Vienna, A-1090 Vienna, Austria; [4]Department of Surgery, Medical University of Vienna, A-1090 Vienna, Austria

Abstract High-grade serous ovarian cancer (HGSOC) is characterized by a *TP53* mutation rate of up to 96.7% and associated with a more aggressive tumor biology. The origin of HGSOC is thought to arise either from fallopian tube secretory cells or the ovarian surface epithelium/inclusion cysts, the former with more evidence. Peritoneal tumor spread is heterogeneous, either excessive in the peritoneum (with miliary appearance) or more confined to the ovaries with only few (bigger and exophytically growing) peritoneal implants. Using RNA sequencing and DNA digital droplet polymerase chain reaction (PCR), we identified two different functional *TP53* mutations in one HGSOC patient: one exclusively in the ovarian tumor mass and the other exclusively in ascites tumor cells, peritoneal tumor masses, and a lymph node metastasis. In blood, both mutations could be detected, the one from the peritoneal tumors with much higher frequency, presumably because of the higher tumor load. We conclude that this mutually exclusive distribution of two different *TP53* mutations in different tumor tissues indicates the development of two independent carcinomas in the peritoneal cavity, probably one originating from a precancerous lesion in the fallopian tube and the other from the ovaries. In addition, in the patient's ascites CD45 and EpCAM, double-positive cells were found—proliferating but testing negative for the above-mentioned *TP53* mutations. This mutually exclusive distribution of two *TP53* mutations is probably further evidence that HGSOC can originate either from the fallopian tube or (more seldom) the ovaries, the former more prone for excessive peritoneal tumor spread.

[Supplemental material is available for this article.]

Corresponding author: dietmar.pils@univie.ac.at

Ontology terms: ovarian neoplasm

Published by Cold Spring Harbor Laboratory Press

doi: 10.1101/mcs.a001461

INTRODUCTION

Mutation of the tumor-suppressor gene *TP53* is regarded as an important driver in cancer onset and progression (Brosh and Rotter 2009). Hence, the structure and function of common mutations have been studied extensively since the discovery of mutation of *TP53*

(Lane and Crawford 1979; Linzer and Levine 1979; Brosh and Rotter 2009). *TP53* is mutated at almost every codon of the DNA binding core domain. Various *TP53* mutations are associated with different penetrance and tumor phenotypes (Olivier et al. 2009). Because of dynamic instability of *TP53* gene mutations, advantageous mutants are clonally selected under tumor promoting conditions (e.g., hypoxia) (Giaccia and Kastan 1998). In serous ovarian carcinoma (SOC), *TP53* mutations are very frequent and occur as an early event (Lee et al. 2007). Particularly, in high-grade serous ovarian cancers (HGSOCs), the mutational frequency can reach up to 96%–96.7% (Ahmed et al. 2010; The Cancer Genome Atlas Research Network 2011) and 99% if an optimized p53 immunohistochemistry is used for detection (Kobel et al. 2016). Loss of wild-type p53 (wt) was shown to confer an aggressive phenotype associated with more aggressive histology (Ahmed et al. 2010) and rapid metastatic dissemination in the peritoneal cavity (Feki and Irminger-Finger 2004). The origin of HGSOC has been under debate since the discovery of "serous tubal intraepithelial carcinomas" (STICs) in patients with hereditary ovarian cancer syndrome (Medeiros et al. 2006; Crum et al. 2007). We recently described two different types of peritoneal tumor spread in HGSOC, one with massive peritoneal involvement (with numerous small millet-sized implants, "miliary") and one with only few larger exophytically growing peritoneal tumor implants (or none at all but with lymph node [LN] involvement) ("nonmiliary") (Auer et al. 2015, 2016b; Bachmayr-Heyda et al. 2016). Both types are different in biological and clinical characteristics, and the miliary type is associated with an unfavorable outcome (Auer et al. 2015; Bachmayr-Heyda et al. 2016). We further demonstrate the first evidence that miliary tumors originate from the fallopian tubes and nonmiliary tumors from ovarian epithelia (Auer et al. 2016a). A gene signature derived from ovarian surface epithelial (OSE) and fallopian tube secretory epithelial (FTE) cells links spread type with putative origin—miliary with tubal and nonmiliary with ovarian origin (Auer et al. 2016a). Recently, the discussion of the exclusive tubal origin of HGSOC was challenged by several publications: Klinkebiel et al. (2016) showed by whole-genome methylation studies that some HGSOC samples are more similar to OSE cells than to FTE cells; Coscia et al. (2016) reported that by using targeted proteomics data, ovarian cancer cell lines can be divided into different clusters, one closer to OSE cells and one closer to FTE cells, and that HGSOC tumor tissues follow this clustering; and Eckert et al. (2016) showed by phylogenetic genomic profiling that STICs are not always the precancerous lesions of HGSOC but can also be secondary implants. Additionally, it was shown that ascites-derived tumor spheroids can implant in the fallopian tube epithelium and thus mimic STIC lesions by ex vivo assays (Eckert et al. 2016).

Here we report a HGSOC patient presenting with two mutually exclusive *TP53* mutations, one restricted solely to the ovarian tumor and the other to the peritoneal tumor masses (including ascites tumor cells and a LN metastasis). We conclude that the patient carries two independent tumors in the peritoneal cavity, distinguishable in their *TP53* mutation signatures, but indistinguishable by histology and the proliferation indices of the tumor cells. In addition, proliferating but not *TP53*-mutated CD45 (a pan-leukocyte marker) and EpCAM (marker for epithelial cells and carcinomas) double-positive cells were detected in the ascites of this patient (Supplemental Information).

RESULTS

Clinicopathological Features of the HGSOC Patient

The patient was diagnosed at the age of 50 with grade three FIGO (Fédération Internationale de Gynécolgie et d'Obstetrique) stage IIIC HGSOC and received debulking surgery with complete macroscopic tumor resection followed by six cycles of adjuvant chemotherapy with carboplatin and paclitaxel together with bevacizumab (starting at the second cycle).

Pathological assessment revealed a bilateral invasive ovarian carcinoma with excessive, widespread invasion of cancer cells within the peritoneal cavity. According to immunohistochemical (IHC) analyses, the characteristic morphology of the tumor comprised of papillary structures—indicative of a serous papillary ovarian carcinoma (adenocarcinoma)—with lymphovascular involvement (L1). Although spreading extensively within the peritoneum, the tumor invasion into the uterus remained small, showed subserous development, and was restricted only to the outer wall of the uterus. The LNs under the serosa were positive. These findings indicated a primary HGSOC, distinguishable from other carcinomas (e.g., endometrial serous carcinoma) (Bartosch et al. 2011). Clinically and according to computer tomography (CT) imaging and cancer antigen (CA125) levels the patient was tumor-free after primary therapy. Bevacizumab maintenance therapy was performed up to 18 cycles, and thereafter the patient had a clinical follow-up every 3 mo in the oncology outpatient department of the Medical University of Vienna. The first recurrence was diagnosed 21 mo after the last dose of platinum chemotherapy and treated with six cycles of carboplatin and pegylated liposomal doxorubicin together with bevacizumab.

IHC staining of the ovarian tumor, peritoneal tumors, and the embedding of ascites cells for various markers was performed to rule out an endometrial serous carcinoma in the peritoneal cavity: Wilms' tumor protein 1 (WT-1), p53, CA125, progesterone receptor (PR), estrogen receptor (ER), vimentin (VIM), and pan-cytokeratin AE1/AE3. Strong expression of WT-1, *p53*, as well as very strong expression of CA125 in tumor cells among all tissues is typical for a high-grade serous carcinoma (Fig. 1). Hormonal receptors showed different expression pattern between the ovarian and the peritoneal tumors: the expression of PR in ovarian tumor cells was heterogeneous but strong. In peritoneal tumors PR was also heterogeneously expressed, but positive cells were only weakly stained. However, ascites tumor cells were PR-negative. In contrast, tumor cells in ascites expressed ER. Tumor cells from ovary and peritoneum showed again very heterogeneous staining for ER. Furthermore, vimentin staining was negative in ovarian, peritoneal, and ascites tumor cells, whereas the pan-cytokeratin AE1/AE3 were positive in tumor cells of ovarian tissue and ascites but showed very diffuse staining in peritoneal tumor cells. Positive expression of vimentin can be allocated to the mesothelial cells. Also, mesothelial cells and leukocytes are positively stained by pan-keratin AE1/AE3. These expression patterns of various histological markers in tumor cells indicated clearly the presence of a high-grade serous papillary ovarian carcinoma with strong positive *p53* expression. Retrospectively, we examined the fallopian tubes in detail and additionally resectioned relevant blocks. Tumor formation appears to originate within ovarian cysts lined with atypical epithelium developing into invasive carcinoma spreading on to the ovarian—and probably the peritoneal—surface. In addition, similar tumor formations were found at the fimbriated extremity of the right fallopian tube in continuity with the local tubal epithelium, indicating the possibility of serous carcinoma originating thereof. However, histopathologically it is not possible to clearly discriminate primary from metastatic tumor tissue in the tubal area because of close proximity and morphologic similarity.

Detection of Two Different *TP53* Mutations in a HGSOC Patient

Routinely, all primary tumor tissues from our tumor tissue bank are analyzed for functional *TP53* mutations using the functional assay of separated alleles in yeast (FASAY) (Deissler et al. 2004). Using ovarian tumor tissue, one mutation in codon 135 (c.404 G>A, C135Y) was found (Table 1; P25; COSMIC accession no. COSP43053). Interestingly, digital droplet polymerase chain reaction (ddPCR) on isolated peritoneal tumor cells revealed no evidence for this mutation in these cells. As we also had RNA-sequencing data of enriched tumor cells from a peritoneal tumor mass of this patient (Auer et al. 2015), we searched mapped reads for a second *TP53* mutation. And indeed, we found reads indicative of a c.581 T>G mutation

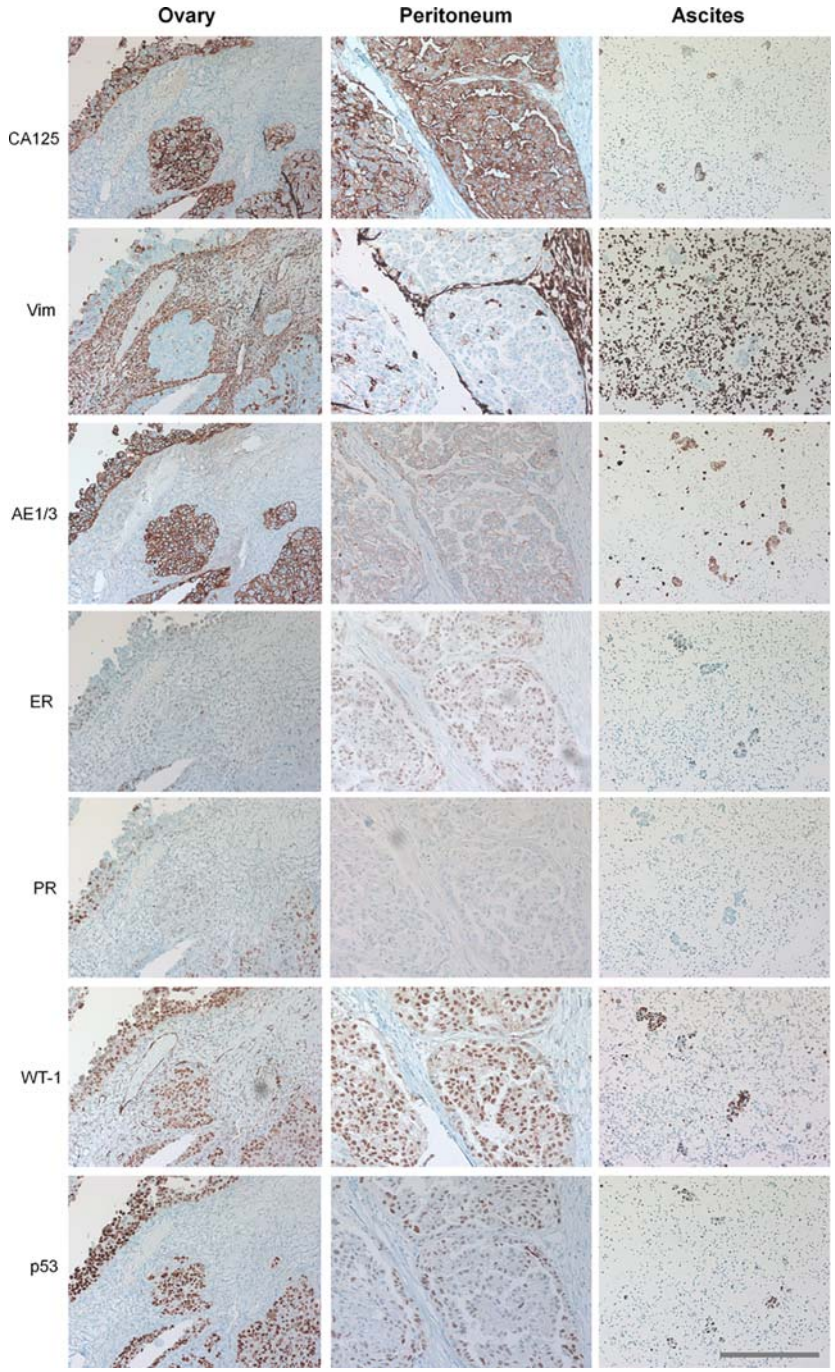

Figure 1. Immunohistochemical staining of the ovarian tumor tissue, a peritoneal tumor tissue, and the embedded ascites cells of the high-grade serous ovarian cancer (HGSOC) patient. Tumor cells are strongly positive for CA125, WT-1, and p53. Whereas vimentin is negative in tumor cells among all tissue types, pan-keratin (AE1/3) is positive in ovarian tumor and aggregated tumor cells in ascites but diffuse-positive in peritoneal tumor. In ovarian and peritoneal tissues, progesterone receptor (PR) and estrogen receptor (ER) expressions in tumor cells are very diffuse and both positive and negative staining of the markers can be detected. In addition, ovarian stroma is positively stained with PR. However, aggregated tumor cells in ascites lack PR expression, whereas ER expression in these cells is positive. Images are visualized with light microscopy. Scale bar, 200 μm at 100× magnification.

Table 1. Variant table

ID	Gene	Chromosome position (hg19)	HGVS cDNA	HGVS protein	HGVS protein Reference	Mutation type	Type	COSMIC ID
P25	*TP53*	17: 7578526	c.404G>A	p.C135Y	NP_001119584.1	Substitution	Somatic	COSP43053
A25	*TP53*	17: 7578268	c.581T>G	p.L194R	NP_001119584.1	Substitution	Somatic	COSP43053

HGVS, Human Genome Variation Society; COSMIC, Catalogue of Somatic Mutations in Cancer; http://cancer.sanger.ac.uk/cosmic.

in exon 6 (L194R) (Table 1; A25; COSMIC accession no. COSP43053). Using this a priori knowledge, Sanger sequencing of this region confirmed this mutation in ascites tumor cells (Fig. 2B).

TP53 Mutational Frequency in SOC

According to the International Agency for Research on Cancer (IARC) *TP53* database (Petitjean et al. 2007) and the Catalogue of Somatic Mutations in Cancer (COSMIC) database (Forbes et al. 2011), 66.0% (804 of 1217) to 78.2% (552 of 706) of all analyzed SOCs have been shown to be mutated. Both identified mutations were infrequent mutants with mutation rates of 0.11 and 0.04, respectively (data from IARC) (Fig. 2A; Petitjean et al. 2007).

The Structure of the p53 Mutations

Next, we analyzed the locations of the two identified *TP53* mutations in the three-dimensional (3D) structure of the protein (Fig. 2D). Both described mutations are located in highly conserved clusters of hotspot mutation regions among different cancers and belong to so-called "buried amino acids," known to be involved in stabilizing protein folding (Cho et al. 1994; Walker et al. 1999). The 3D structure of the DNA binding core domain of wt p53 shows that the two mutations are located in regions of important secondary structure domains. The "ovarian *TP53* mutation" C135Y (P25; c.404 G>A mutation in exon 5) causes the alteration of a nucleophilic cysteine to an aromatic tyrosine at codon 135, which is located in the S2′ sheet region of the loop–sheet–helix motif. The C135Y (c.404 G>A) mutation was described as a protein destabilizing mutant (Cho et al. 1994). This mutant was also reported to exhibit a loss of function and interferes with wt p53 if wt p53 is present, but showed gain-of-function mutation in the absence of wt p53 (Dearth et al. 2007).

The "peritoneal *TP53* mutation" L194R (A25; c.581 T>G mutations in exon 6) causes the replacement of a hydrophobic leucine with a basic arginine in the L2 loop of the protein, also described as the protein–DNA interaction stabilizing loop. This mutant is also characterized to cause a loss of function (Jordan et al. 2010) because of its specific location near the zinc binding region. Structurally analyzed, both mutations are localized at protein stabilizing regions of p53, which can result in disturbed protein function.

Distribution of Two Independent *TP53* Mutations in HGSOC

Sequencing analysis of the HGSOC patient showed two differentially distributed mutations: one mutation C135Y (c.404 G>A), identified by the FASAY assay in the ovarian tumor mass (P25) and another L194R (c.581 T>G) mutation detected in a peritoneal tumor mass (A25), initially from RNA-sequencing data and verified by Sanger sequencing in ascites tumor cells (Fig. 2B).

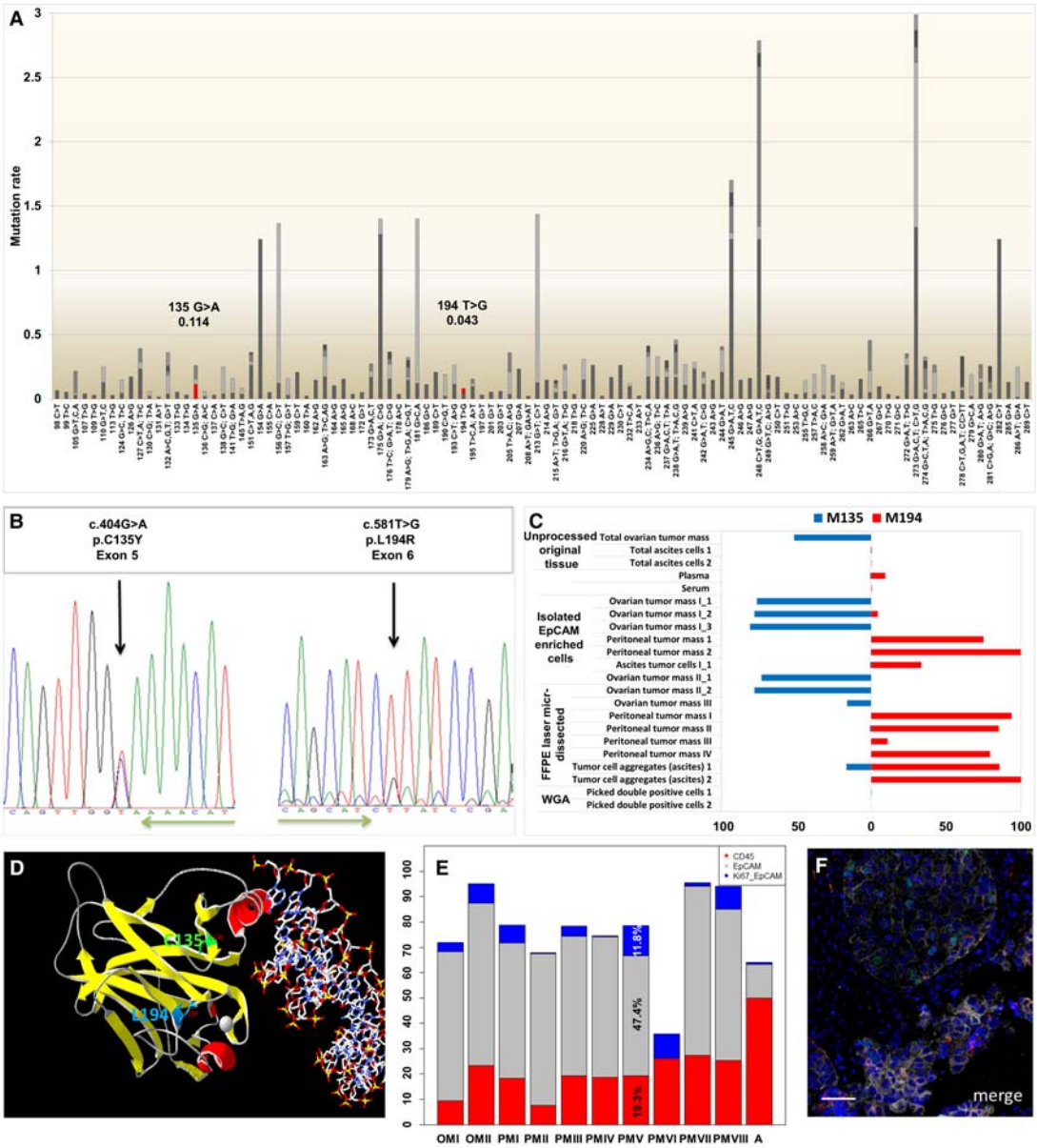

Figure 2. (*A*) Mutational frequency in the DNA binding domain of *p53* in epithelial ovarian cancers: only missense mutations in the DNA binding domain were considered and analyzed, comprising 217 mutations from 658 in total. All indels, nonsense mutations, splice variants, frameshifts, and silent mutations were excluded. Six mutations outside the DNA binding domain were removed (International Agency for Research on Cancer [IARC] *TP53* database, Petitjean et al. 2007). (*B*) Sequencing of the *TP53* gene of the patient. The sequencing revealed the presence of two different mutations. (*C*) *TP53* mutation analyses of ovarian masses, isolated ascites cell aggregates, and four different peritoneal implants from appendix vermiformis (I), omentum majus (II and IV), and diaphragm (III). Different ovarian tumor masses, peritoneal tumor masses, and ascites, as well as spheroids, are indicated in Roman numerals (I–IV) and experiment repeats are denoted in Arabic numerals (1–3). WGA, whole-genome amplification. (*D*) Three-dimensional structure of the DNA binding core domain of wild-type p53 with highlighted ovarian C135Y-p53 (green) and peritoneal L194R-p53 mutations (blue). The mutation at codon L194R localized in the L2 loop (labeled in blue), which supports the L3 loop, occurred mainly in peritoneal tumor masses. The C135Y mutation in the S2′ β-sheet at loop–helix–sheet motif (labeled in green) was shown to be a thermosensitive mutation. PDB ID: 4HJE (Chen et al. 2013). Structures were created using Swiss-PdbViewer v4.1 (Guex Nicolas et al. 2012). (*E*) Immunofluorescence (IF) quantification of immune and tumor cells. Expression levels of *CD45*-positive immune cells (red) and EpCAM-positive tumor cells (gray) in ovarian masses (OMs), in different peritoneal masses (PMs) from appendix vermiformis (I), omentum majus (II and IV), diaphragm (III, VII), LN (data is shown on the graph) implant in mesocolon (V), ligamentum falciforme (VI), and Douglas pouch (VIII) and in ascites (A). Ki67 staining of tumor cells indicates the proliferation indices of tumor cells (blue). (*F*) IF staining of ovarian mass. The merged image of IF staining shows *p53* (green), CD45 (red), EpCAM (white), and Ki67 (yellow). The cell nuclei were counterstained with DAPI. The images were visualized with fluorescence microscopy at 200× magnification. Scale bar, 50 µm.

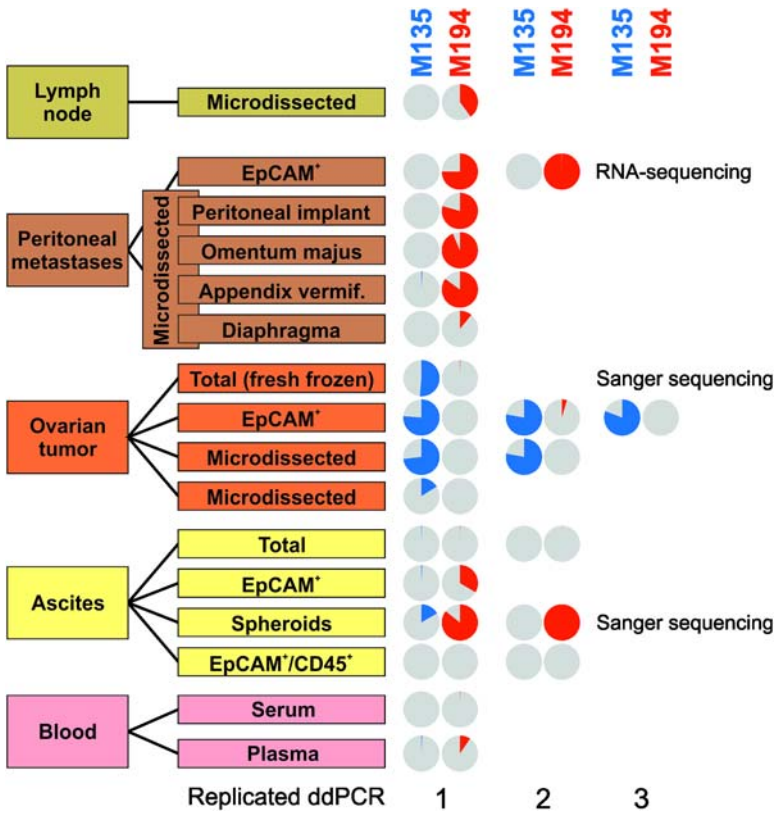

Figure 3. Scheme of samples and performed analyses. Pie charts represent the relative frequencies of the corresponding mutation (in blue the ovarian [i.e., C135Y (c.404 G>A)] and in red the peritoneal [i.e., L194R (c.581 T>G)] mutation).

Using ddPCR, we analyzed ratios of these two different mutations from different regions of the ovarian tumor, from different peritoneal tumor implants and ascites tumor cells using DNA isolated from diverse sample types (fresh frozen total tissues, ascites cells, enriched tumor cells, free DNA from serum and plasma, formalin-fixed paraffin-embedded [FFPE] sections, and picked single cells). The C135Y (c.404 G>A) mutation was found exclusively in the ovarian tumor mass, whereas the L194R (c.581 T>G) mutation was solely detected in the peritoneal tumor masses and ascites tumor cells, which confirmed the Sanger and massively parallel RNA-sequencing results. Both mutations showed very high mutational frequencies in the corresponding tissues (Fig. 3): a median of 76.2% (range, 16.0%–80.8%; interquartile range [IQR], 15.6; $N = 7$) for the C135Y (c.404 G>A) mutation in the ovarian tumors and a median of 82.2% (range, 11.1%–85.1%; IQR, 24.9; $N = 4$) for the L194R (c.581 T>G) mutation in the peritoneal implants and ascites (Figs. 2C, 3). Interestingly, the malignant LN from the mesocolon showed the same mutation as the peritoneal tumor masses.

Tumor cell aggregates (spheroids, isolated from fresh ascites) mainly contained the "peritoneal mutation" L194R (c.581 T>G), but also the "ovarian mutation" C135Y (c.404 G>A), albeit in a much lower frequency (Figs. 2C, 3) (in average 93.0% vs. 8.3%). In plasma of the patient, both mutations L194R (c.581 T>G) and C135Y (c.404 G>A) were detected in low levels (9.5% and 0.7%, respectively). In serum, only 0.4% of the L194R (c.581 T>G) mutation was detected, but no C135Y (c.404 G>A) mutation (Figs. 2C, 3).

Measuring the Proliferation Indices of Cells with Different *TP53* Mutations

To assess dependence of tumor cell proliferation on the two different *TP53* mutations, the proliferation index of tumor cells was determined by IF nuclear Ki67 staining in the ovarian (Fig. 2F), as well as the peritoneal tumor tissues and the embedded ascites cells.

The ovarian and the peritoneal tumor tissues contained a median of 60.4% (range, 8.2%–71.9%; IQR, 7.6; $N = 10$) tumor cells and about a median of 19.2% (range, 7.6%–27.7%; IQR, 6.4; $N = 10$) immune cells (Fig. 2E). IF staining with Ki67 revealed that among all ovarian and peritoneal tumor tissues a median of 5.5% (range, 0.2%–11.8%; IQR, 6.6; $N = 10$) of tumor cells and a median of 0.19% (range, 0.004%–0.19%; IQR, 0.9; $N = 10$) of immune cells were proliferating. Only the peritoneal tumor mass from the ligamentum falciforme consisted of mostly fat cells and very few tumor cells (8.2%) with a very high proliferation rate of 89.0%. In ascites, the majority of cells were immune cells (43.3%–50.0%), of which 1.19%–1.48% were proliferating and 11.2%–15.6% of ascites cells were tumor cells, of which ~0.9% were proliferating. In addition, 6.5% of total $CD45^+/EpCAM^+$ double-positive cells (6.2%–9.2%) were proliferating (Supplemental Table S1). We found that the proliferation indices of tumor cells varied substantially among all analyzed tissues (median, 3.8%; range, 0.2%–11.8%; IQR, 7.1; $N = 12$) but did not depend on a specific mutation, indicating that the two different *p53* mutations did not determine proliferation rates.

DISCUSSION

Here we report a remarkable finding in a patient with HGSOC with excessive widespread tumor invasion in the peritoneal cavity: mutation analyses revealed two different functional *TP53* mutations, one exclusively in the ovarian tumor mass and the other exclusively in ascites tumor cells and tumor masses from the peritoneal cavity. We conclude that the mutually exclusive signature of the two mutations indicates two independent tumor populations. The dominant "peritoneal mutation" L194R (c.581 T>G) populated the ascites and spread within the peritoneal cavity, compared with the "ovarian mutation" C135Y (c.404 G>A), found nearly exclusively in the ovarian primary tumor. Some tumor aggregates (spheroids) in the ascites also showed the "ovarian mutation," indicating that cells from the ovarian tumor can shed off and remain floating in the ascites (forming spheroids or as single cells). Moreover, the LN metastasis showed the "peritoneal mutation," indicating that the lymph system was infiltrated by tumor cells from either ascites tumor cells or peritoneal tumor implants rather than from the main primary ovarian tumor.

Hoogstraat et al. reported a DNA and RNA-sequencing study of ovarian serous adenocarcinoma that revealed two different independent *TP53* missense mutations in one patient at distinct tumor locations, including the ovary and the peritoneum. The authors suggested that the differently mutated tumor regions constitute two independent tumors or very early branched subclones (Hoogstraat et al. 2014). The latter is implausible, as it is thought that HGSOC mainly derives from premalignant lesion in the fallopian tube, with *TP53* mutations as one of the first driver mutations.

The analysis of the mutation structure revealed that both mutations showed high mutational frequencies in the corresponding tissues and are localized at protein stabilizing regions of p53, which can result in a disturbed protein function.

We detected less free-circulating DNA in the serum of the patient compared with plasma. This is in concordance with the literature reporting less total free-circulating DNA in plasma (Jackson et al. 2016), but relatively more from the tumor (i.e., mutated), compared with serum containing more total free-circulating DNA but relatively less from the tumor. The higher concentration of the "peritoneal mutation" L194R (c.581 T>G) in free-circulating

DNA in plasma and serum is probably due to the much higher tumor load from peritoneal tumor implants and ascites tumor cells than from the ovarian tumor.

Shortcomings

Contamination with PCR products from previous *TP53* mutation analyses can be nearly completely excluded as both mutations were new in our laboratory at the time of analysis and both mutations were analyzed several times weeks apart and analyzed by different people. The peritoneal mutation was also analyzed from a lavage of the uterine cavity, which was taken completely independently from surgery and analyzed by different people including targeted DNA sequencing (Maritschnegg et al. 2015). We can also exclude the possibility of swap of tissues or samples to explain all results, as both mutations were each proven in tissues we collected (i) directly from the operating room, (ii) from fresh material different people from our laboratory got from pathology on the day of surgery, and (iii) as FFPE blocks from the pathology weeks after the surgery. Furthermore, to ensure the assignment of both mutations to the patient, short tandem repeat analyses (STR-PCR), which we usually use to confirm cell line identities, confirmed the identity of blood-derived genomic DNA with the DNA of the ovarian tumor mass and from ascites cells.

Origin of HGSOC?

In a series of publications we recently introduced two modes of peritoneal tumor spread in HGSOC, miliary and nonmiliary, with numerous biological, immunological, and outcome differences between them (Auer et al. 2015, 2016b; Bachmayr-Heyda et al. 2016). We have further evidence that miliary tumors arise from the fallopian tubes and nonmiliary from the ovaries (Auer et al. 2016a): comparative transcriptome analysis links these two distinct metastatic phenotypes, miliary and nonmiliary, with putative origin of HGSOC tubes and the ovaries. Further evidence for (rare) cases of HGSOC of ovarian origin comes from methylome studies (Klinkebiel et al. 2016), targeted proteomics (Coscia et al. 2016), and phylogenetic genomics (Eckert et al. 2016). Even secondary tumor implants in the fallopian epithelium can mimic STICs (Eckert et al. 2016). But there is also evidence by identical *TP53* mutations for clonal relations of STICs and pelvic tumor masses, at least in pelvic carcinosarcomas with HGSOC involvement (Ardighieri et al. 2016). McDaniel et al. described two cases of *BRCA1/2* mutated HGSOC patients with concordant STIC and ovarian tumor mass TP53 mutations (McDaniel et al. 2015). Nevertheless, we believe the finding in this patient (i.e., two mutually exclusive distributed functional *TP53* mutations) is further evidence that HGSOC can originate from tissues outside the ovaries (from the fallopian tubes or the peritoneum) but also from the ovaries (indistinguishable from histopathologic presentation) and that the former are more prone for peritoneal tumor spread (therefore probably presenting differently clinically). Both characteristics, tumor spread and putative origin, are also correlated to different outcomes (Auer et al. 2015, 2016a,b; Bachmayr-Heyda et al. 2016; Coscia et al. 2016) and therefore should be considered more intensely in HGSOC treatment and targeted therapy research.

METHODS

Patient Sample Collection

During the primary surgery, tumor masses from ovaries and several peritoneal tumor masses (from the omentum majus, appendix vermiformis, ligamentum falciforme, Douglas pouch, diaphragm, and a LN implant in the mesocolon), as well as ascites containing tumor cells, were obtained and processed further for analysis.

Preparation of Ovarian and Peritoneal Tissues

Ovarian and peritoneal tissues, obtained during surgery, were immediately stored in buffered growth medium (Dulbecco's modified Eagle's medium [DMEM] [Life Technologies] + 10 mM HEPES, pH 7.2 [Sigma-Aldrich]). Tissues were cut into small pieces and digested by Liberase DH (0.26 U/ml) in DMEM (10 mM HEPES, pH 7.2) for 60 min at 37°C gently stirring. The reaction was stopped by adding 10 µl of fetal calf serum. The cell suspension was filtered through a filter with 40-µm mesh size and rinsed with DMEM supplemented with 4 mM ethylenediaminetetraacetic acid (EDTA) (Sigma-Aldrich). The cells were centrifuged at 120*g* for 10 min and the pellet was washed twice in phosphate-buffered saline (PBS) (total tissue). The cells were resuspended in 1 ml DMEM and either cryostored in liquid nitrogen (addition of 5% dimethylsulfoxide [DMSO] [Sigma-Aldrich] to growth medium) or prepared immediately for cell enrichment as described below (Table 2).

Preparation of Ascites Cells

Cell aggregates (here referred to as spheroids) and single cells from the ascites were separated using 30-µm (the retentate contained spheroids) and 20-µm filters (the flow through contained single cells) (BD). The filters (Partec CellTrics) were washed once with 1× phosphate-buffered saline (PBS). The spheroids were collected from the 30-µm filter by inverting the filter and washing the membrane with 5 ml prewarmed DMEM. Single cells were collected in DMEM (Life Technologies) containing 0.4 mM EDTA (Sigma-Aldrich). After

Table 2. Sample preparation overview

Sample names	Origin	Preparations and methods
Total ovarian tumor mass	Right ovary	Original tissue
Ovarian tumor mass I (1–3)	Right ovary	Total EpCAM-enriched cells
Ovarian tumor mass II (1–2)	Right ovary, random 1	Microdissected from FFPE
Ovarian tumor mass III (1–2)	Right ovary, random 2	Microdissected from FFPE
Total ascites cells (1–2)	Peritoneum	Total cell content of ascites
Ascites tumor cells	Peritoneum	Total EpCAM-enriched cells
Tumor cell aggregates (ascites) (1–2)	Peritoneum	Spheroids microdissected from FFPE
Picked double-positive cells (1–2)	Peritoneum	Picked $EpCAM^+/CD45^+$ cells
Peritoneal tumor mass (1–2)	Random tissue implant	Total EpCAM-enriched cells
Peritoneal tumor mass I	Omentum majus	Microdissected from FFPE, IF
Peritoneal tumor mass II	Appendix vermiformis	Microdissected from FFPE, IF
Peritoneal tumor mass III	Diaphragma	Microdissected from FFPE, IF
Peritoneal tumor mass IV	Random tissue	Microdissected from FFPE, IF
Peritoneal tumor mass V	LN in mesocolon	Microdissected from FFPE, IF
Peritoneal tumor mass VI	Ligamentum falciforme	Microdissected from FFPE, IF
Peritoneal tumor mass VII	Diaphragma	Microdissected from FFPE, IF
Peritoneal tumor mass VIII	Douglas pouch	Microdissected from FFPE, IF
Plasma	Blood	Total free-circulating nucleic acid
Serum	Blood	Total free-circulating nucleic acid

All patient materials were provided directly from the operating room or from the pathology. The processed ovarian tumor masses, peritoneal tumor masses, and ascites preparations (biological replicates) are indicated in roman numerals (I–VIII) and repeated experiments (technical replicates) are labeled with Arabic numerals in brackets. Preparation methods reveal various strategies used in quantification of cells or validation of mutational analysis.
FFPE, formalin-fixed, paraffin-embedded; IF, immunofluorescence.

centrifugation at 400*g* for 10 min, both spheroids and single cell pellets were washed twice in PBS and resuspended in cell-free ascites supernatant containing 5% DMSO (Sigma-Aldrich) for freezing.

Preparation of FFPE Tissue Slides

FFPE tissue blocks from ovarian (right ovary) and peritoneal tumor masses as well as ascites cell blocks from agarose were prepared according to the standard procedure. Prepared tissue sections of 4 µm were first deparaffinized for 60 min at 58°C, with subsequent incubation in Xylol, 2× for 5 min. For rehydration, the tissue sections were incubated in descending alcohol concentrations as follows: 2 × 100% each 3 min, 1 × 96% for 1 min, 1 × 80% for 1 min, and 1 × 70% for 1 min.

FFPE Tissue Sections for Microdissection

FFPE tissue sections for microdissection were prepared on membrane slides to micro-dissect areas with predominantly tumor cells with the mmi CellCut laser system (MMI).

Isolation of DNA from Total Tissue Pellet, FFPE Tissue Sections, and EpCAM-Enriched Tumor Cells from Ascites

Genomic DNA from the total tissue pellets, FFPE tissue sections (including ovarian tumor mass and four different peritoneal implants) and with magnetic beads enriched $CD45^+$ or $EpCAM^+$ cells from ascites were isolated using QIAamp QIAGEN FFPE DNA kit protocol from FFPE tissue sections (QIAGEN). 2 × 12 µl DNA was eluted in ATE buffer at RT. ddPCR was performed with obtained DNA (Hindson et al. 2011).

DNA Extraction from Plasma and Serum

Plasma and serum were centrifuged at 4600*g* for 15 min at 4°C. DNA extraction from plasma and serum was performed according to QIAamp circulating nucleic acid protocol for 1 ml serum and 4 ml plasma (QIAGEN). Of note, 40 ng/µl of amplified DNA was analyzed by ddPCR (Bio-Rad) as described.

Immunohistochemical

IHC staining of the ovarian tumor, peritoneal tumors and the embedded ascites cells was conducted according to the standard protocol for following markers: WT-1, p53, CA125, PR, ER, vimentin, and pan-cytokeratin AE1/AE3.

Immunofluorescence

Multicolor IF staining of FFPE tissue sections from patient materials were first deparaffinized and rehydrated as described above. Heat-induced epitope retrieval was performed by heating up the slides in EDTA pH 8.0 (1:50 EDTA in distilled water) using a microwave (850 W for 2.5 min, followed by 160 W for 13 min). After cooling down the buffer slowly to room temperature (RT), slides were washed two times in PBS for 3 min each. The slides were blocked with Ultra V Block (Thermo Fisher Scientific) for 7 min. After rinsing, the slides were treated with primary antibodies (diluted in DAKO antibody diluent with background reducing components) in appropriate concentrations for 45–60 min at RT in a humidity chamber. IF staining with the following primary antibodies was performed on FFPE tissue sections: anti-*CD45* (dilution 1:1000, source rat, isotype IgG2b, clone orb96558, Biorbyt), anti-*CD45* (dilution 1:1500, source rabbit, isotype IgG, clone E19-G, DB Biotech), anti-*EpCAM* (dilution 1:300,

source mouse, isotype IgG1, clone VU1D9, Cell Signaling) and anti-*EpCAM* (dilution 1:300, source rabbit, isotype IgG, clone E144, Abcam), anti-*CD16* (dilution 1:50, source mouse, isotype IgG2a, clone 2H7, Thermo Scientific), anti-*CD14* (dilution 1:250, source rabbit, isotype IgG, clone EPR3653, Novus Biologicals), anti-*p53* (dilution 1:125, source mouse, isotype IgG2a, clone DO-1, Merck Millipore), anti-pan-cytokeratin (Ck) 8, 18, 19 (dilution 1:200, source mouse, isotype IgG1, clone A45-B/B3, AS Diagnostics), anti-*CD44* (dilution 1:1000, source mouse, isotype IgG2a, clone 156–3C11, Cell Signaling) and anti-Ki67 (dilution 1:400, source rabbit, isotype IgG1, clone MIB-1, Dako).

After 3× washing in PBS supplemented with 0.1% Tween (PBS-T) for 3 min, the slides were incubated with secondary antibodies for 30–60 min, prepared in 6% bovine serum albumin in PBS. For detection of both panels, the following fluorescence-labeled goat secondary antibodies were used at a 1:1000 dilution: Alexa Fluor 555 anti-rat, Alexa Fluor 647 anti-mouse IgG1, Alexa Fluor 488 anti-mouse IgG2a, and Alexa Fluor 750 anti-rabbit (Life Technologies). For negative controls, FLEX Ready-to-Use Mouse Negative Control containing a cocktail of mouse IgG_1, IgG_{2a}, IgG_{2b}, IgG_3, and IgM (DAKO Autostainer/Autostainer Plus) was used. The slides were washed again in PBS three times and the nuclei were counterstained with DAPI for 5 min. The tissue sections were mounted with Fluoromount-G (Southern Biotech). The positively stained cell components were scanned with TissueFAXS fluorescence microscopy (TissueGnostics) and laser scanning microscopy (Zeiss, LSM-700) (Fig. 2F).

Quantification of cells was performed using the automated cell analyzing software CellProfiler v.2.1.1 (Carpenter et al. 2006). The CellProfiler analysis pipeline is available in the Supplemental Material.

TP53 Mutation Detection and Conformational Sequencing

Total RNA from fresh frozen tissue of the patient was analyzed for functional *TP53* mutations according to the FASAY assay (Deissler et al. 2004). *TP53* mutations were confirmed by Sanger sequencing according to a standard sequencing protocol described elsewhere (Sliutz et al. 1997).

Digital Droplet PCR

Genomic DNA prepared with different sample-dependent methods was used for ddPCR analysis. A 20 µl reaction mix was prepared: 20 ng genomic DNA, 2× ddPCR Supermix (Bio-Rad), 40× duplexed *p53*/codon153 or *p53*/codon194 TaqMan system. The following primer and probe sets were used (Applied Biosystems, Life Technologies): c.581 T>G, L194R (23 bp FW: CACTGATTGCTCTTAGGTCTGGC; 22 bp RV: GTCATCCAAATA CTCCACACGC; 15 bp: FAM-CTCAGCATCGTATCC-MGB; 15 bp: VIC-CTCAGCATCTTAT CC-MGB) and c.404 G>A, C135Y (27 bp FW: AACTCTGTCTCCTTCCTCTTCCTACAG; 19 bp RV: CTGCACAGGGCAGGTCTTG; 21 bp: FAM-TCAACAAGATGTTTTACCAA C-MGB; 19 bp: VIC-AACAAGATGTTTTGCCAAC-MGB).

The PCR was performed with 10 min initial denaturation at 95°C followed by 40 cycles consisting of denaturation for 30 sec at 94°C, annealing and extension for 60 sec at 60°C, and a final 10 min inactivation step at 98°C by means of thermal cycler (Eppendorf). PCR products were quantified with the QX100 Droplet Digital PCR system (Bio-Rad). Positive controls with known mutations were used in order to evaluate reliability of mutation quantification using Quantasoft (Bio-Rad).

The *TP53* mutation analysis depends on a two color fluorescence detection of FAM and VIC fluorescence channels. After thresholds were set using the positive control samples, concentrations of mutated and wt alleles were calculated.

ADDITIONAL INFORMATION

Data Deposition and Access

The mutations are accessible from the COSMIC database (http://cancer.sanger.ac.uk/cosmic) under accession no. COSP43053.

Ethics Statement

The patient signed an informed consent for participation and publication of this study and approval for this study was obtained from the ethical review board at the Medical University of Vienna (no. 793/2011).

Acknowledgments

We thank the Vienna Campus Support Facility (CSF) NGS Unit for performing the Illumina Next Generation Sequencing. Further thanks go to Barbara Holzer and Eva Schuster for performing the functional FASAY *p53* assay and *TP53* Sanger sequencing and to Eva Obermayr for supporting us by cell picking.

Author Contributions

N.S., A.B.-H., K.A., S.A., and D.P. designed the study. N.S., A.B.-H., K.A., S.A., and S.D. processed clinical samples. A.B.-H. performed RNA sequencing, S.A. did the clinical review and provided clinical samples, R.H. did the pathological review, D.P. performed bioinformatics, N.S., K.A., A.B., S.A., and D.P. analyzed and interpreted the data, and all contributed to and approved the final version of the manuscript.

Funding

This work was supported by funds of the Oesterreichische Nationalbank (Anniversary Fund, project number: 14595) and The Austrian Science Fund (FWF) project no. P28137.

Competing Interest Statement

The authors have declared no competing interest.

Referees

James D. Brenton
Anonymous

Received September 13, 2016; accepted in revised form March 31, 2017.

REFERENCES

Ahmed AA, Etemadmoghadam D, Temple J, Lynch AG, Riad M, Sharma R, Stewart C, Fereday S, Caldas C, Defazio A, et al. 2010. Driver mutations in *TP53* are ubiquitous in high grade serous carcinoma of the ovary. *J Pathol* **221:** 49–56.

Ardighieri L, Mori L, Conzadori S, Bugatti M, Falchetti M, Donzelli CM, Ravaggi A, Odicino FE, Facchetti F. 2016. Identical *TP53* mutations in pelvic carcinosarcomas and associated serous tubal intraepithelial carcinomas provide evidence of their clonal relationship. *Virchows Arch* **469:** 61–69.

Auer K, Bachmayr-Heyda A, Aust S, Sukhbaatar N, Reiner AT, Grimm C, Horvat R, Zeillinger R, Pils D. 2015. Peritoneal tumor spread in serous ovarian cancer—epithelial mesenchymal status and outcome. *Oncotarget* **6:** 17261–17275.

Auer K, Bachmayr-Heyda A, Aust S, Grunt TW, Pils D. 2016a. Comparative transcriptome analysis links distinct peritoneal tumor spread types, miliary and non-miliary, with putative origin, tubes and ovaries, in high grade serous ovarian cancer. *Cancer Lett* **388:** 158–166.

Auer K, Bachmayr-Heyda A, Sukhbaatar N, Aust S, Schmetterer KG, Meier SM, Gerner C, Grimm C, Horvat R, Pils D. 2016b. Role of the immune system in the peritoneal tumor spread of high grade serous ovarian cancer. *Oncotarget* **7:** 61336–61354.

Bachmayr-Heyda A, Auer K, Sukhbaatar N, Aust S, Deycmar S, Reiner AT, Polterauer S, Dekan S, Pils D. 2016. Small RNAs and the competing endogenous RNA network in high grade serous ovarian cancer tumor spread. *Oncotarget* **7:** 39640–39653.

Bartosch C, Manuel Lopes J, Oliva E. 2011. Endometrial carcinomas: a review emphasizing overlapping and distinctive morphological and immunohistochemical features. *Adv Anat Pathol* **18:** 415–437.

Brosh R, Rotter V. 2009. When mutants gain new powers: news from the mutant *p53* field. *Nat Rev Cancer* **9:** 701–713.

Carpenter EA, Jones TR, Lamprecht MR, Clarke C, Kang IH, Friman O, Guertin DA, Chang JH, Lindquist RA, Moffat J, et al. 2006. CellProfiler: image analysis software for identifying and quantifying cell phenotypes. *Genome Biol* **7:** R100.

Chen Y, Zhang X, Dantas Machado AC, Ding Y, Chen Z, Qin PZ, Rohs R, Chen L. 2013. Structure of *p53* binding to the BAX response element reveals DNA unwinding and compression to accommodate base-pair insertion. *Nucleic Acids Res* **41:** 8368–8376.

Cho Y, Gorina S, Jeffrey PD, Pavletich NP. 1994. Crystal structure of a *p53* tumor suppressor–DNA complex: understanding tumorigenic mutations. *Science* **265:** 346–355.

Coscia F, Watters KM, Curtis M, Eckert MA, Chiang CY, Tyanova S, Montag A, Lastra RR, Lengyel E, Mann M. 2016. Integrative proteomic profiling of ovarian cancer cell lines reveals precursor cell associated proteins and functional status. *Nat Commun* **7:** 12645.

Crum PC, Drapkin R, Miron A, Ince TA, Muto M, Kindelberger DW, Lee Y. 2007. The distal fallopian tube: a new model for pelvic serous carcinogenesis. *Curr Opin Obstet Gynecol* **19:** 3–9.

Dearth RL, Qian H, Wang T, Baroni TE, Zeng J, Chen SW, Yi SY, Brachmann RK. 2007. Inactive full-length *p53* mutants lacking dominant wild-type *p53* inhibition highlight loss of heterozygosity as an important aspect of *p53* status in human cancers. *Carcinogenesis* **28:** 289–298.

Deissler H, Kafka A, Schuster E, Sauer G, Kreienberg R, Zeillinger R. 2004. Spectrum of *p53* mutations in biopsies from breast cancer patients selected for preoperative chemotherapy analysed by the functional yeast assay to predict therapeutic response. *Oncol Rep* **11:** 1281–1286.

Eckert AM, Pan S, Hernandez KM, Loth RM, Andrade J, Volchenboum SL, Faber P, Montag A, Lastra R, Peter ME, et al. 2016. Genomics of ovarian cancer progression reveals diverse metastatic trajectories including intraepithelial metastasis to the fallopian tube. *Cancer Discov* **6:** 1342–1351.

Feki A, Irminger-Finger I. 2004. Mutational spectrum of *p53* mutations in primary breast and ovarian tumors. *Crit Rev Oncol Hematol* **52:** 103–116.

Forbes AS, Bindal N, Bamford S, Cole C, Kok CY, Beare D, Jia M, Shepherd R, Leung K, Menzies A, et al. 2011. COSMIC: mining complete cancer genomes in the Catalogue of Somatic Mutations in Cancer. *Nucleic Acids Res* **39:** D945–D950.

Giaccia JA, Kastan MB. 1998. The complexity of *p53* modulation: emerging patterns from divergent signals. *Genes Dev* **12:** 2973–2983.

Guex Nicolas AD, Peitsch MC, Schwede T. 2012. *Swiss-PdbViewer*. S. I. o. B. (SIB).

Hindson JB, Ness KD, Masquelier DA, Belgrader P, Heredia NJ, Makarewicz AJ, Bright IJ, Lucero MY, Hiddessen AL, Legler TC, et al. 2011. High-throughput droplet digital PCR system for absolute quantitation of DNA copy number. *Anal Chem* **83:** 8604–8610.

Hoogstraat M, de Pagter MS, Cirkel GA, van Roosmalen MJ, Harkins TT, Duran K, Kreeftmeijer J, Renkens I, Witteveen PO, Lee CC, et al. 2014. Genomic and transcriptomic plasticity in treatment-naïve ovarian cancer. *Genome Res* **24:** 200–211.

Jackson BJ, Choi DS, Luketich JD, Pennathur A, Stahlberg A, Godfrey TE. 2016. Multiplex preamplification of serum DNA to facilitate reliable detection of extremely rare cancer mutations in circulating DNA by digital PCR. *J Mol Diagn* **18:** 235–243.

Jordan JJ, Inga A, Conway K, Edmiston S, Carey LA, Wu L, Resnick MA. 2010. Altered-function *p53* missense mutations identified in breast cancers can have subtle effects on transactivation. *Mol Cancer Res* **8:** 701–716.

Klinkebiel D, Zhang W, Akers SN, Odunsi K, Karpf AR. 2016. DNA methylome analyses implicate fallopian tube epithelia as the origin for high-grade serous ovarian cancer. *Mol Cancer Res* **14:** 787–794.

Kobel M, Piskorz AM, Lee S, Lui S, LePage C, Marass F, Rosenfeld N, Mes Masson AM, Brenton JD. 2016. Optimized p53 immunohistochemistry is an accurate predictor of *TP53* mutation in ovarian carcinoma. *J Pathol Clin Res* **2:** 247–258.

Lane PD, Crawford LV. 1979. T antigen is bound to a host protein in SV40-transformed cells. *Nature* **278:** 261–263.

Lee Y, Miron A, Drapkin R, Nucci MR, Medeiros F, Saleemuddin A, Garber J, Birch C, Mou H, Gordon RW, et al. 2007. A candidate precursor to serous carcinoma that originates in the distal fallopian tube. *J Pathol* **211:** 26–35.

Linzer ID, Levine AJ. 1979. Characterization of a 54K dalton cellular SV40 tumor antigen present in SV40-transformed cells and uninfected embryonal carcinoma cells. *Cell* **17:** 43–52.

Maritschnegg E, Wang Y, Pecha N, Horvat R, Van Nieuwenhuysen E, Vergote I, Heitz F, Sehouli J, Kinde I, Diaz LA Jr, et al. 2015. Lavage of the uterine cavity for molecular detection of Mullerian duct carcinomas: a proof-of-concept study. *J Clin Oncol* **33:** 4293–4300.

McDaniel AS, Stall JN, Hovelson DH, Cani AK, Liu CJ, Tomlins SA, Cho KR. 2015. Next-generation sequencing of tubal intraepithelial carcinomas. *JAMA Oncol* **1:** 1128–1132.

Medeiros F, Muto MG, Lee Y, Elvin JA, Callahan MJ, Feltmate C, Garber JE, Cramer DW, Crum CP. 2006. The tubal fimbria is a preferred site for early adenocarcinoma in women with familial ovarian cancer syndrome. *Am J Surg Pathol* **30:** 230–236.

Olivier M, Petitjean A, Marcel V, Petre A, Mounawar M, Plymoth A, de Fromentel CC, Hainaut P. 2009. Recent advances in *p53* research: an interdisciplinary perspective. *Cancer Gene Ther* **16:** 1–12.

Petitjean A, Mathe E, Kato S, Ishioka C, Tavtigian SV, Hainaut P, Olivier M. 2007. Impact of mutant *p53* functional properties on *TP53* mutation patterns and tumor phenotype: lessons from recent developments in the IARC *TP53* database. *Hum Mutat* **28:** 622–629.

Sliutz G, Schmidt W, Tempfer C, Speiser P, Gitsch G, Eder S, Schneeberger C, Kainz C, Zeillinger R. 1997. Detection of *p53* point mutations in primary human vulvar cancer by PCR and temperature gradient gel electrophoresis. *Gynecol Oncol* **64:** 93–98.

The Cancer Genome Atlas Research Network. 2011. Integrated genomic analyses of ovarian carcinoma. *Nature* **474:** 609–615.

Walker RD, Bond JP, Tarone RE, Harris CC, Makalowski W, Boguski MS, Greenblatt MS. 1999. Evolutionary conservation and somatic mutation hotspot maps of *p53*: correlation with *p53* protein structural and functional features. *Oncogene* **18:** 211–218.